Determination of interfacial thermal resistance at the nanoscale

Lin Hu, Tapan Desai, and Pawel Keblinski

Phys. Rev. B **83**, 195423 — Published 10 May 2011

DOI: 10.1103/PhysRevB.83.195423

Determination of interfacial thermal resistance at nanoscale

Lin Hu[1], Tapan Desai[2] and Pawel Keblinski[1*]

[1]*Department of Materials Science and Engineering, Rensselaer Polytechnic Institute, Troy, New York 12180, USA*

[2]*Advanced Cooling Technologies, Inc., Lancaster, Pennsylvania, Lancaster, PA 17601, USA*

Using molecular dynamics simulations and model graphene layers in an organic matrix we demonstrate that interfacial thermal resistance determined via "*thermal relaxation method*" is up to an order of magnitude larger than that determined from "*direct simulation method*" of heat transfer across the matrix-graphene-matrix interface. We provide an explanation of this difference based on the spectral analysis of the frequency dependent vibrational temperature. The importance of our finding lies in the fact that the *relaxation method* mimics experimental laser based pump-probe measurements of the interfacial thermal resistance, while the *direct simulation method* provides information relevant to predicting and understanding thermal conductivity of nanocomposites.

*Corresponding author email: keblip@rpi.edu

I. Introduction

In the presence of the heat flux normal to the interface a discontinuous temperature drop, ΔT, develops due to the mismatch in phonon spectrum of the materials forming the interface. The associated interfacial resistance, also called the Kapitza resistance [1], R_K, or equivalently the interfacial thermal conductance $G_K = 1/R_K$, is quantified via

$$J_Q = -G_K \Delta T \qquad (1)$$

where J_Q is the heat flux across the interface. The importance of the interfacial resistance can be most easily gauged via a concept of the Kapitza length (l_K), i.e., the equivalent thickness of a bulk material forming the interface that has the same overall thermal resistance as the interface. E. g., for water thermal conductivity of 0.6 W/m-K and a typical thermal conductance for hydrophilic interface of G_K = 100 MW/m^2-K [2], a Kapitza length of l_K = 6 nm is obtained. However, for carbon nanotubes in water, G_K can be as low as 10 MW/m^2-K [3] leading to l_K = 60 nm. The interfacial thermal resistance is particularly important in nanostructured materials due to the high density of interfaces. For example, the thermal conductivity of carbon nanotube-polymer nanocomposites is severely limited by the interfacial resistance [4].

Direct determination of the value of the interfacial thermal resistance between nanoparticles and the surrounding media is conducted via transient absorption experiments [5]. In such experiments, the thermal energy is "pumped" in to nanoparticles by laser light and then the nanoparticle thermal relaxation rate is "probed" via optical measurements. When the thermal relaxation process is limited by the interfacial thermal resistance, the nanoparticle temperature relaxes to the temperature of the media in an

exponential manner. The associated relaxation time constant, τ, is related to the interfacial conductance via [4]

$$\tau = \frac{C}{AG_K} \tag{2}$$

where C is the heat capacity of nanoparticle and A is the area of the nanoparticle.

In this article, using molecular dynamics simulations and a model of a graphene layer embedded in an organic matrix material, we demonstrate that the value of the interfacial thermal resistance determined by the thermal relaxation method is several times larger than the value obtained by the direct simulation method of heat flow across the matrix-graphene-matrix interface. The latter value is relevant to the determination of the thermal conductivity of nanocomposites.

II. Model structures and simulation methodology

Our main model structure is presented in the top panel of Fig. 1. In the center of the structure there is a block of 3 graphene sheets in the A-B-A stacking sequence, sandwiched in amorphous organic matrix composed of phenol formaldehyde chains with 8 repeating units in the ortho-ortho sequence and a methyl group termination [6]. The choice of such complex organic matrix material is due its importance for ablative thermal protection. However, in the context of this study we note that the thermal transport properties of the matrix are typical of an organic material. The surface area parallel to the sheets has the dimensions, 25.56 Å $\times$ 24.60 Å. Periodic boundary conditions were applied in all three dimensions and the size of the simulation cell in the normal direction was adjusted to about 120 Å such that the phenolic resin density was 1.25 gm/cc. The phenolic chains were not cross-linked and no chemical bonds existed between the

graphene and the matrix. In order to assess possible size effects, in several cases, we studied structures with 4 times larger cross-sectional area, and found that within the statistical error the results are the same as for the original structure.

The above described structure was employed in thermal relaxation simulations and heat source/sink simulations. The heat source/sink simulations were performed with two source/sink strategies. First, the heat source was placed on graphene and the heat sink in the organic matrix (see Fig. 1, top panel). Second, both the heat source and sink was placed in the organic matrix (see Fig. 3, top panel). For the latter case, we doubled the structure in the cross plane direction leading to 2 graphene layers sandwiched between two regions of organic matrix. In addition to the structure with graphene layer consisting of 3 planes, we examined structures with 1 and 5 planes, respectively.

The interatomic interactions were described by the Polymer Consistent Force Field (PCFF) [7] and time step of 0.25 fs was used in all simulations. Such small time steps is due to explicit presence of hydrogen atoms in the model and the requirement of high-level of energy conservation. After energy minimization, we heated each structure to 1000 K at constant volume, equilibrated at this temperature for 200 ps and cooled down to 300 K. We followed up with 200 ps equilibration at 300 K and constant pressure of 1 atm.

In the thermal relaxation studies, we increased "instantaneously" the temperature of the graphene layers in the equilibrated structure to 650 K by scaling velocities of each graphene atom by the same factor, and allowed the system to thermally relax at constant energy and volume. This setup mimics experimental pump-probe approach, where the energy is delivered to nanoparticles over a fraction of a picoseconds which is typically

much shorter than the thermal relaxation time. We also note that the energy injection to the system in MD simulations is similar to the experimental situation since in both cases the bulk of the energy is injected into high frequency phonons. In MD simulations we inject energy to all modes uniformly, however, vast majority of the thermal energy (heat capacity) is in high-energy modes, as their density is far larger than the low frequency modes in graphene (also see Fig. 4). In experiment photon laser energy is ~ 1 eV and is mostly injected via electron-phonon coupling to high-energy optical modes.

In the heat source/sink simulations after equilibration at 300 K and 1 atm, we follow up with constant volume and energy simulations, however, we placed a heat source at the graphene and two heat sinks in the matrix at the edges of simulation cell. The heat source and sinks were applied by rescaling the atomic velocities by a uniform factor for each atom in heat source/sink region such that the heat power delivered/removed was the same each time step. The power of the source was equal to the combined power of the sinks, such that the total energy of the system remained constant. After a steady state was established, we monitored time averaged temperature profiles, where the temperature is defined via equipartition theorem from average kinetic energy, as shown in the bottom panel of Fig. 1. From the temperature profile we can evaluate the interfacial conductance and thermal conductivity of the matrix. In the structures with two graphene layers we placed both the heat source and sink regions in the center of the two matrix regions.

In our simulations we used constant power (heat flux) sink and source where each time step we added/removed the same and relatively small energy, of 3.5×10^{-23} J . To examine a potential role of the thermostat details on the results, most importantly on the interfacial thermal resistance, we performed simulations with velocity rescaling constant

temperature thermostats for the case of single graphene plane structure. The interfacial conductance for constant temperature thermostats was 8.9 MW/m^2-K, which is very close to 8.6 MW/m^2-K value obtained with constant energy thermostats. In the case of constant temperature thermostats, the thermal power delivered to graphene at each time step fluctuated between positive and negative values with an amplitude over two orders of magnitude larger that the average power. Consequently the perturbation of the atomic motion was dramatically larger than in the case of constant power thermostats. The fact that the results are almost identical for two significantly different thermostats demonstrates independence of the results on the thermostat details.

III. Results and discussion

The temperature vs. time plot of the thermally relaxing graphene averaged over 5 independent runs are shown in Fig. 2. The initial rapid temperature drop (not shown) is associated with the redistribution of kinetic and potential energy within graphene. The following relaxation process is associated with heat transfer from the graphene to the matrix. The thermal relaxation process fits very well to the exponential decay (see Fig. 2). The resulting relaxation time is 115 ps which, according to Eq. 2, gives the interfacial thermal conductance G_K = 21 MW/m^2-K. This value is similar to that obtained for carbon nanotube – octane interface via MD simulations and in pump-probe experiments on carbon nanotube - organic surfactant - water interface [3].

The interfacial conductance of 21 MW/m^2-K is relatively small and can significantly limit thermal conductivity of a composite material. To illustrate the relative role of the interfacial thermal conductance on overall thermal transport we preformed steady state,

heat source-sink simulations. In this simulation, a constant heat power is delivered to the graphene by rescaling atomic velocities and heat is removed from the edge of the simulation cell at the same rate. After a short transient a steady state temperature profile is established as shown in Fig. 1. From the temperature gradients in the organic matrix (phenolic resin) we evaluated its bulk thermal conductivity value to be 0.15 W/m-K, which is typical for an amorphous polymeric material. The most prominent feature in the temperature profile, in Fig. 1, is a very large temperature drop at the graphene – phenolic resin interface, which indeed dominates the overall temperature drop across the whole simulation cell. This drop gives the value of interfacial conductance via Eq. 1 to be G_K = 20 MW/m^2-K, which is very close to the value obtained in thermal relaxation simulations.

Based on the relaxation and steady state simulations described above one would conclude that interfacial thermal resistance is very important and can significantly limit the thermal conductivity of graphene-organic matrix composites. However, in contrast to the simulations described above and pump-probe measurements, where the heat is delivered directly to the graphene layer, in the composite applications the relevant situation is when heat simply crosses the layer. To capture this situation, we performed simulations on a structure with two graphene layers separated by two phenolic resin slabs (see. Fig. 3). In this case the both heat sink and source are placed in the matrix. The steady state temperature profile presented in Fig. 3 shows much lower temperature drops at the matrix-graphene interfaces. This leads to a strikingly different conclusion to that derived from prior simulations, namely that in the graphene organic matrix composites the interfacial thermal resistance has a negligible effect on the composite conductivity. In

fact, based on the small interfacial temperature drop indicated in Fig. 3 we estimated the interfacial conductance, G_K = 170 ± 20 MW/ m^2-K. This value is an order of magnitude larger than that obtained in relaxation and steady state simulations, where the heat source was placed in the graphene layer.

In the above estimate of the interfacial thermal conductance, we evaluated the temperature drop at the graphene-matrix interface by taking ½ of the offset between the linear temperature profiles in the adjacent matrix regions, labeled ΔT in Fig. 3. This gives an effective conductance of the interface. An alternative definition will be an actual temperature drop at each interface, indicated as $\Delta T'$ in Fig. 3. Since $\Delta T' > \Delta T$ the corresponding conductance is lower and has value of G'_K = 80 ± 10 MW/ m^2-K. In either case, the conductance is much larger than that derived form the relaxation or steady state simulations (20 MW/ m^2-K) with the heat source placed on graphene.

Furthermore, in the case of 1 and 5 graphene plane layers with heat source and sink placed in the resin the conductance, evaluated from $\Delta T'$ temperature drop, is 110 and 85 MW/m^2-K, respectively. These values for interfacial conductance are large and similar to that obtained from the 3 plane layer case. The situation is somewhat different when the source is on graphene. For a single graphene plane layer, the conductance is only 10 MW/m^2-K and for 5 graphene layer the conductance is 25 MW/m^2-K. These results strongly indicate a trend: the conductance is small for small number of planes, and the conductance increases with increasing number of planes. This behavior is consistent with the fact that in the limit of a large number of planes, the interfacial conductance should be independent from the placement of the heat source and sink and will represent the conductance of the interface between resin and macroscopic graphite.

In all cases of nanoscopic graphene layers studies we observe that the conductance of the graphene organic matrix interface is much larger when the heat source and sink are not placed on graphene. To understand the origin of this huge difference between the interfacial thermal conductance values evaluated by the different methods, we calculated the Fourier transform (FT) of the velocity autocorrelation function (VAF) for a carbon atom residing in the graphene layer, which is representative all C atoms forming graphene. We calculated FT of the VAF (separately for in-plane and out-of-plane motion) for an equilibrium (EQ) system held at 300 K (see Fig. 4) and for the steady state, non-equilibrium, (NE) system where graphene is the heat source (Fig. 1). FT of the VAF is proportional to the vibrational density of states (VDOS) [8] and is also proportional to the square of the average velocity. This via the equipartition theorem allows to determine the frequency, *f*, dependent temperature of the vibrational modes of the non-equilibrium system, T_{NE}, from [9],

$$T_{NE}(f) = T_{EQ}\frac{VDOS_{NE}}{VDOS_{EQ}} \qquad (3)$$

where T_{EQ} in the temperature of the equilibrium system.

The frequency dependent temperature is plotted in Fig. 5 for the in-plane and out-of-plane motion. While the high frequency temperature is about the same as the overall graphene temperature, in the low frequency regime (0-10 Thz) the temperature is much lower and much closer to the temperature of the adjacent phenolic resin. In here, we define overall temperature as that given by the average kinetic energy. The majority of the modes are in the high frequency region. Consequently, the overall temperature is dominated by the temperature of those modes.

The data presented in Fig. 5 clearly indicate that low frequency modes in graphene are strongly coupled with the matrix, while high frequency modes are not. This implies that the heat transfer between graphene and the matrix is dominated by low frequency modes, which have much lower temperature difference with the adjacent matrix, than the high frequency modes.

To further illustrate the heat source placement dependent energy transfer in heated graphene layer, we performed steady state simulations on 5 plane model with the heat source placed on a single, central graphene, as shown in top panel of Fig. 6. The resulting temperature profile is shown in bottom panel of Fig. 6. Several distinct temperature drops can be identified. The most pronounced drop is between the heated central plane and the two adjacent planes, labeled as ΔT". The associated interfacial conductance is 23 MW/m^2-K. The temperature drop between adjacent to central planes and outer planes is much lower (ΔT' in Fig. 6) and the corresponding conductance is 74 MW/m^2-K. This indicates that frequency dependent energy distribution in various planes is different leading to associated differences in effective thermal conductance. The interfacial conductance corresponding to the temperature difference between the outer planes and the phenol resin is 41 MW/m^2-K. This value is about twice larger than that obtained when heat source was acting on all 5 planes. This is another manifestation of a trend where away from the source, the effects of the source on the interfacial conductance diminish and the intrinsic heat source independent behavior can manifest itself.

The above observations combined with the fact that low frequency modes dominate thermal transport across the interface can explain the discrepancy between interfacial thermal conductances obtained by different simulations setups. In the simulations, where

the graphene is the heat source, the interfacial resistance has two main contributions: (i) the internal to graphene resistance between high frequency modes (that have the majority of thermal energy) and low frequency modes and (ii) external resistance between low frequency modes in graphene (that carry most heat across the interface) and the matrix. When the heat sources and sinks are outside graphene, the internal resistance plays no role in interfacial thermal transport and in effect the interfacial conductance is much higher. In the case of 5 plane graphene layer with the central plane heat source, the resistance between the central and adjacent planes is high due to the majority of thermal energy being pumped into "non-conductive" high frequency modes. However, the spectral distribution of energy supplied to the adjacent planes is already filtered by the interface and is likely in better local equilibrium. In consequence, the interfacial conductance between adjacent and outer planes is much higher.

IV. Summary and conclusion.

In summary, we used MD simulations of graphene in a organic matrix structure to demonstrate that the interfacial thermal resistance determined from thermal relaxation processes can be very different from the one relevant to predicting and understanding thermal conductivity of nanoscale composites [10]. While our findings seem surprising, they are analogous to thermal relaxation processes associated with spectral analysis of molecules. In such analysis, a particular high frequency mode is exited by laser (e.g. OH stretch in water [11]). The following thermal relaxation is understood in terms of intra-molecular cascade of thermal energy to lower frequency vibrations before final dissipation into the media via low frequency modes [12]. Also, the fact that graphene

exhibits relatively smaller interfacial thermal resistance with organic media can explain the better thermal performance of graphite nanoplatelets than carbon nanotubes in polymer nanocomposites [13].

The above observations combined with the fact that low frequency modes dominate thermal transport across the interface can explain the discrepancy between interfacial thermal conductance obtained by different simulations setups. In the simulations where the graphene is the heat source the interfacial resistance has two main contributions: (i) the internal to graphene resistance between high frequency modes (that have the majority of thermal energy) and low frequency modes and (ii) external resistance between low frequency modes in graphene (that carry most heat across the interface) and the matrix. When the heat sources and sinks are outside graphene the internal resistance plays no role in interfacial thermal transport and in effect the interfacial conductance is much higher.

This work was supported by the U.S. Air Force Office of Scientific Research Grant No. MURI FA9550-08-1-0407 and by the NASA Small Business Innovation Research Grant (SBIR), under Contract No. NNX10CC69P.

References:

[1] E. T. Schwartz and R. O. Pohl, *Rev. Mod. Phys*. **61**, 605 (1989).

[2] Z. B. Ge, D. G. Cahill, and P. V. Braun, Phys. Rev. Lett. **96** 186101 (2006).

[3] S. T. Huxtable, D. G. Cahill, S. Shenogin et. al., Nat. Mater. **2**, 731 (2003).

[4] S. Shenogin, L. Xue, R. Ozisik, P. Keblinski, and D. G. Cahill, J. Appl. Phys. **95**, 8136 (2004).

[5] O. M. Wilson, X. Hu, D. G. Cahill, and P. V. Braun, Phys. Rev. B **66**, 224301 (2002).

[6] D.E. Jiang, A.C.T. van Duin, W.A. Goddard and S. Dai, J. Phys. Chem. A **113**, 6891 (2009).

[7] H. Sun, S. J. Mumby, J. R. Maple, and A. T. Hagler, J. Am. Chem. Soc. **116**, 2978 (1994).

[8] M. P. Allen and D. J. Tildesley, Computer Simulation of Li- quids (Clarendon, Oxford, 1989).

[9] N. Shenogina, P. Keblinski, S. Garde, J. Chem. Phys. **129**, 155105 (2008).

[10] T.C. Clancy , S.J.V. Frankland, J.A. Hinkley, T.S. Gates, Int. J. Therm. Sci. **49** (2010).

[11]A. J. Lock, H. J. Bakker, J. Chem. Phys. **117**, 1708 (2002).

[12] P. Li, J. T. Sage, P. M. Champion, J. Chem. Phys. **97**, 3214–3227 (1992).

[13] A. P. Yu, P. Ramesh, M. E. Itkis, E. Bekyarova, R. C. Haddon, J. Phys. Chem. C **111**, 7565 (2007).

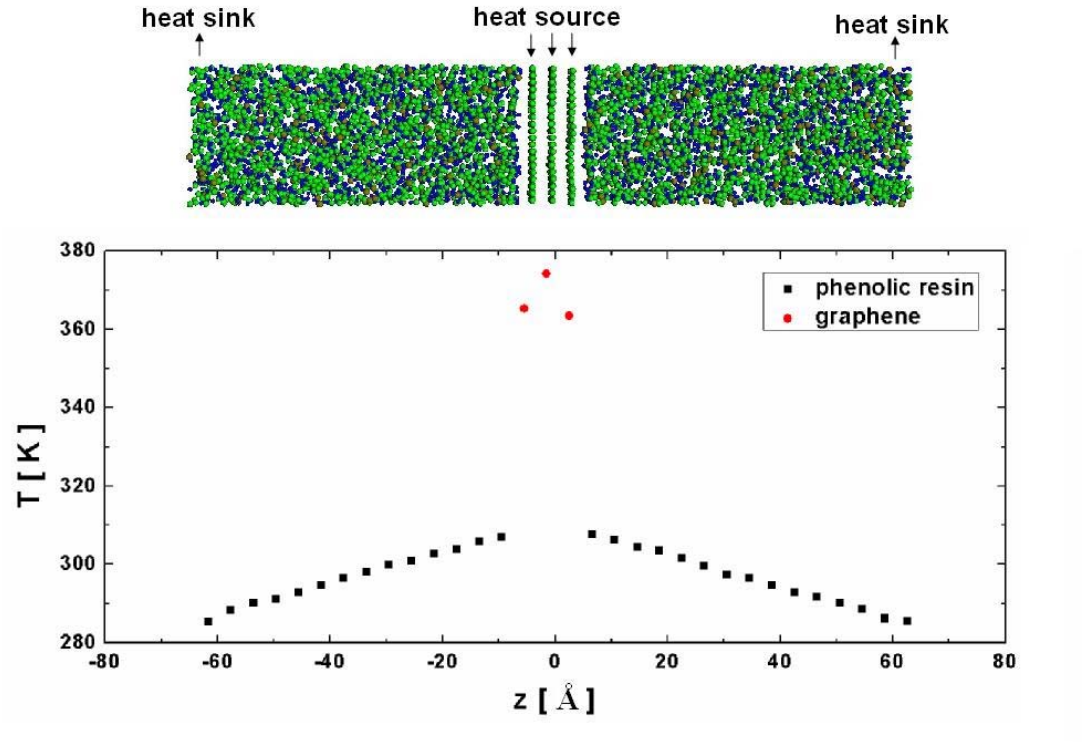

FIG. 1: (Color on line) Top panel: Model structure with a graphene layer in phenolic resin. Bottom panel: The steady state temperature profile obtained from non-equilibrium, heat source-sink method, with graphene constituting the heat source.

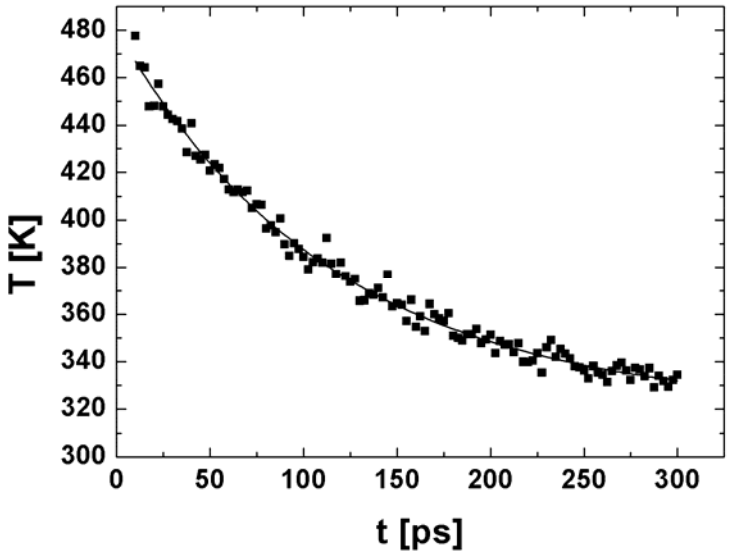

FIG. 2: Graphene layer temperature in thermal relaxation simulations mimicking pump-probe thermal measurements. The line represents an exponential relaxation fit in the 10-300 ps range.

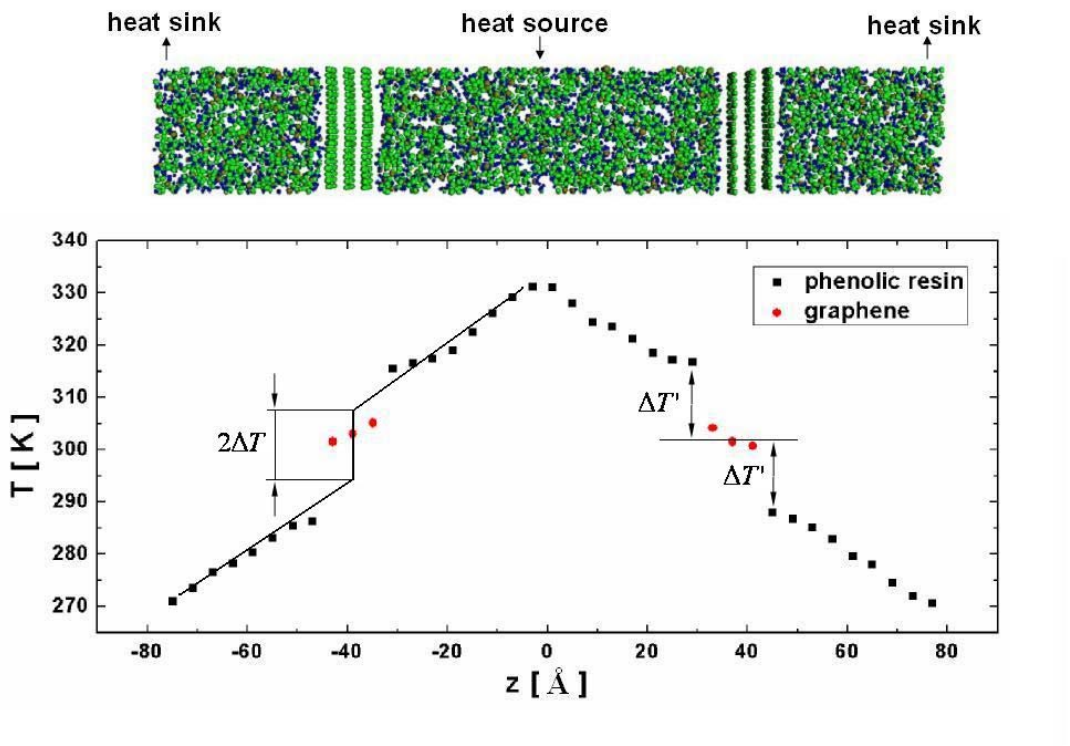

FIG. 3: (Color on line) Top panel: Model structure with two graphene layers. Bottom panel: The steady state temperature profile obtained from non-equilibrium simulations with both heat source and sink placed in the phenolic resin. Two different definition of the interfacial temperature drop are indicated as ΔT and ΔT'.

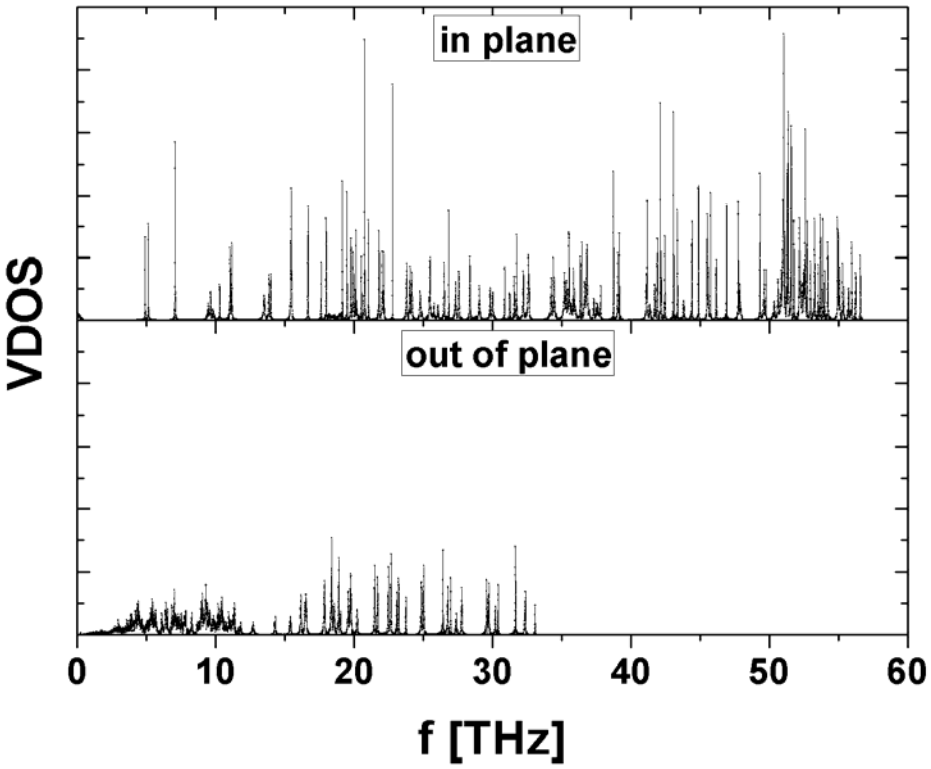

FIG. 4: Top panel: Graphene carbon atom vibrational density of states (VDOS) for in plane motion. Bottom panel: The same for out of plane motion.

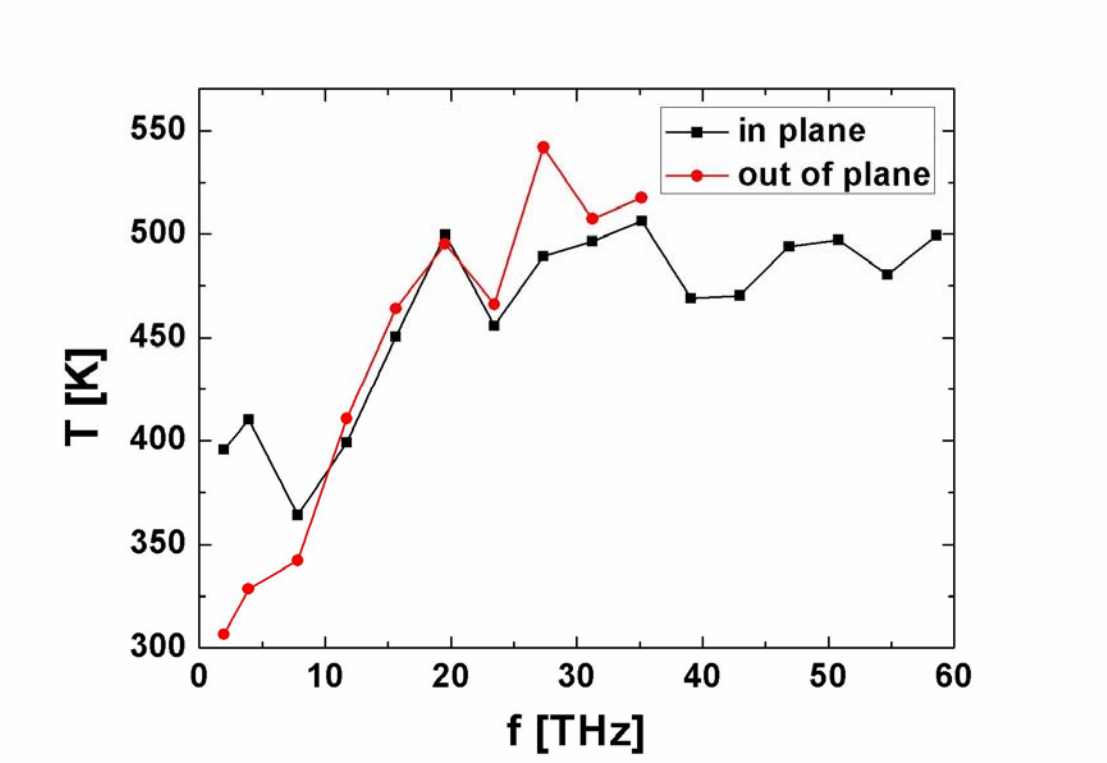

FIG. 5: (Color on line) In plane and out of plane temperature of graphene as a function of frequency for steady state simulations with heat source located at graphene (see Fig. 1).

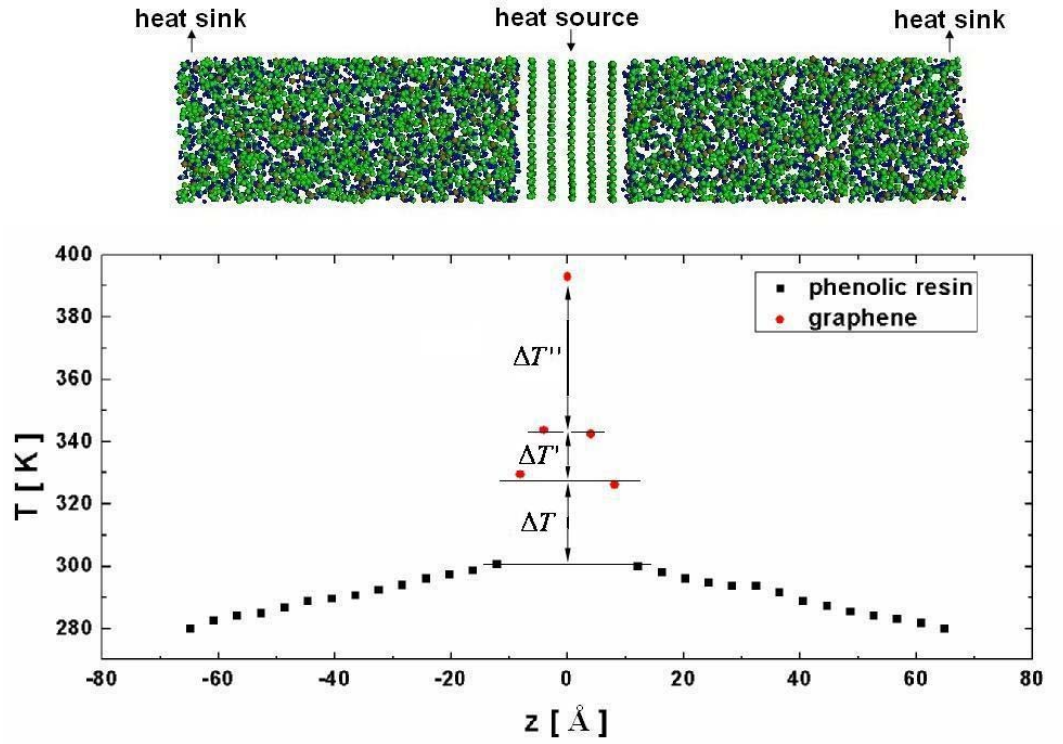

FIG. 6: (Color on line) Top panel: Model structure with a graphene layer in phenolic resin. Bottom panel: The steady state temperature profile obtained from non-equilibrium, heat source-sink method, with the central graphene plane constituting the heat source. Various temperature drops discussed in text are indicated.